Chapter

Surface-Enhanced Raman Scattering: Introduction and Applications

Samir Kumar, Prabhat Kumar, Anamika Das and Chandra Shakher Pathak

Abstract

Scattering of light by molecules can be elastic, Rayleigh scattering, or inelastic, Raman scattering. In the elastic scattering, the photon's energy and the state of the molecule after the scattering events are unchanged. Hence, Rayleigh scattered light does not contain much information on the structure of molecular states. In inelastic scattering, the frequency of monochromatic light changes upon interaction with the vibrational states, or modes, of a molecule. With the advancement in the laser sources, better and compact spectrometers, detectors, and optics Raman spectroscopy have developed as a highly sensitive technique to probe structural details of a complex molecular structure. However, the low scattering cross section (10^{-31}) of Raman scattering has limited the applications of the conventional Raman spectroscopy. With the discovery of surface-enhanced Raman scattering (SERS) in 1973 by Martin Fleischmann, the interest of the research community in Raman spectroscopy as an analytical method has been revived. This chapter aims to familiarize the readers with the basics of Raman scattering phenomenon and SERS. This chapter will also discuss the latest developments in the SERS and its applications in various fields.

Keywords: Raman scattering, surface-enhanced Raman spectroscopy, enhancement factor, nanoparticles, 2D materials

1. Introduction: Raman scattering

Scattering of light by molecules can be elastic, *Rayleigh scattering*, or inelastic, *Raman scattering*. In the elastic case, the photon's energy and the state of the molecule after the scattering events are unchanged. Hence, Rayleigh scattered light does not contain much information on the structure of molecular states [1]. In inelastic scattering, the frequency of photons of monochromatic light changes upon interaction with the vibrational states, or modes, of a molecule. The effect was postulated theoretically by Smekal et al. in 1923 but was first discovered experimentally by C.V. Raman in 1928 in an experiment using the sun as a light source [2–4].
In Raman scattering, two inelastic processes can occur:

- *Stokes* process: An incident photon $h\nu_0$ excites a molecular vibration $h\nu_{vib}$ and is thus scattered with the corresponding difference in energy $h(\nu_0 - \nu_{vib})$ (red shift).

- *Anti-Stokes* process: The photon acquires vibrational energy and is scattered with a higher energy $h(\nu_0 + \nu_{vib})$ (blue shift).

This shift provides information about vibrational, rotational, and other low-frequency transitions in molecules. Raman spectroscopy can be used to study solid, liquid, and gaseous samples.

1.1 Classical theory of the Raman effect

Raman scattering can be explained using the molecular polarizability [5]. If a molecule is placed in an electric field, electrons and nuclei get displaced. Due to the separation of charged species, an electric dipole moment is induced in the molecule, and it is said to be polarized. If E is the strength of the electric field and μ is the magnitude of the induced dipole moment, then

$$\mu = \alpha E \tag{1}$$

where α is the polarizability of the molecule. If a sample is subjected to an electromagnetic wave of frequency ν, the electric field experienced by each molecule of the sample varies as

$$E = E_0 \cos 2\pi\upsilon t \tag{2}$$

where E_0 is the amplitude of the electromagnetic wave. From Eq. (1)

$$\mu = \alpha E_0 \cos 2\pi\upsilon t \tag{3}$$

Thus, Eq. (3) implies that interaction of electromagnetic radiation of frequency ν induces a molecular dipole moment that oscillates and emits radiation of the same frequency, and this is the classical explanation of Rayleigh scattering. However, the ability to perturb the local electron cloud of a molecular structure depends on the relative location of the individual atoms; hence, the polarizability is a function of the instantaneous position of the constituent atoms. So, the polarizability changes with small displacement from equilibrium position (i.e., molecular vibration) and is given by

$$\alpha = \alpha_0 + \left(q - q_{eq}\right)\frac{\partial \alpha}{\partial q} \tag{4}$$

where α_0 is equilibrium polarizability and q_{eq} and q are bond lengths at equilibrium position and any instant, respectively. If a molecule executes simple harmonic motion, the displacement can be represented as

$$q - q_0 = q_{max} \cos 2\pi\upsilon_{vib} t \tag{5}$$

where ν_{vib} is the vibrational frequency of a molecule and q_{max} is the maximum separation distance between atoms relative to their equilibrium position. Substituting Eq. (5) into Eq. (4) gives

$$\alpha = \alpha_0 + \left(\frac{\partial \alpha}{\partial q}\right) q_{max} \cos 2\pi\upsilon_{vib} t \tag{6}$$

Substituting Eq. (6) into Eq. (3) gives

$$\mu = E_0 \cos 2\pi\upsilon t \left[\alpha_0 + \left(\frac{\partial\alpha}{\partial q}\right) q_{max} \cos 2\pi\upsilon_{vib} t\right] \tag{7}$$

or

$$\mu = \alpha_0 E_0 \cos 2\pi\upsilon t + E_0 \left(\frac{\partial\alpha}{\partial q}\right) q_{max} \cos 2\pi\upsilon t \ \cos 2\pi\upsilon_{vib} t \tag{8}$$

or

$$\mu = \alpha_0 E_0 \cos 2\pi\upsilon t + \frac{E_0}{2} q_{max} \left(\frac{\partial\alpha}{\partial q}\right) \cos\left[2\pi(\upsilon - \upsilon_{vib})t\right] + \frac{E_0}{2} q_{max} \left(\frac{\partial\alpha}{\partial q}\right) \cos\left[2\pi(\upsilon + \upsilon_{vib})t\right] \tag{9}$$

The first term in Eq. (9) represents Rayleigh scattering and occurs at the excitation frequency ν. The second and third terms correspond to Stokes ($\nu - \nu_{vib}$) and anti-Stokes ($\nu + \nu_{vib}$) scattering. In both inelastic scatterings, the excitation frequency is modulated by the vibrational frequency of the bond.

Besides, from Eq. (9), the molecules that have Raman-active vibration modes must experience a change in polarizability during a vibration $\left(\frac{\partial\alpha}{\partial q}\right)$, i.e., the electron density in the molecule must distort from its typical shape (inducing a dipole). Molecules with symmetrical bends and stretches, therefore, are generally better Raman scatterers. So, for a molecule to be Raman active, its molecular rotation or vibration must cause a change in a component of molecular polarizability.

1.2 Quantum theory of the Raman effect

Raman scattering can be easily understood in terms of the quantum theory of radiation. In the quantum model, the molecules exist in quantized energy levels corresponding to possible stationary states of the molecule. When radiation having an energy $h\nu$ incident on a sample, it is considered that the photons undergo collisions with the molecules. When the collision is elastic, the photons will be

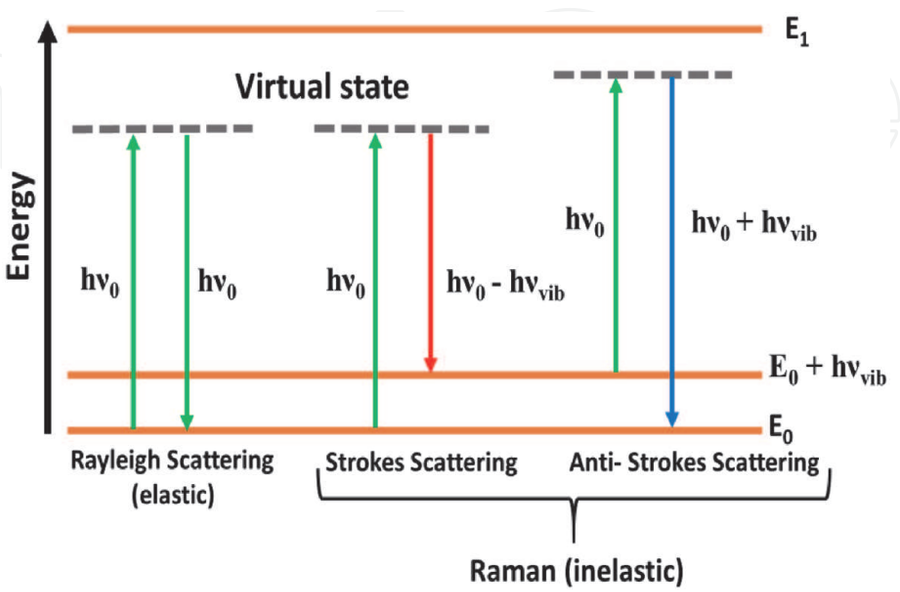

Figure 1.
Energy level diagram for Rayleigh and Raman scattering, where $\Delta E = h\nu_{vib}$ *represents the difference in vibration energy levels [7].*

deflected unchanged, but it is also possible that during the collision, energy is exchanged between the photon and molecule, and as a result, the molecule can gain or lose energy ΔE, where $\Delta E = h\nu_{vib}$ represents a difference in the vibrational or rotational energy levels of that molecule [6]. In quantum mechanical terms, the scattering can be considered as an excitation to a virtual state lower in energy than a real electronic state. When the molecule gains energy ΔE, the photon will be scattered with energy $h\nu - h\nu_{vib}$, and the scattering is known as Stokes' scattering. Conversely, if the molecule loses energy ΔE, the scattered photon will have energy $h\nu + h\nu_{vib}$, and this type of scattering is known as anti-Stokes' scattering. Generally, Stokes' radiation is stronger than the anti-Stokes' radiation. **Figure 1** illustrates the energy level diagram for scattering [7].

2. Surface-enhanced Raman spectroscopy

One of the limitations of the Raman effect is that it is a very weak phenomenon. About one in 10^7 photons undergo Raman scattering. Therefore the Raman signal is very low from low concentrations of the analyte or poor Raman scatterers. Sometimes the high fluorescence from the molecule obscures the Raman signals. Surface-enhanced Raman spectroscopy (SERS) is all about amplifying Raman signals from molecules, by several orders of magnitude [8]. SERS is a technique where molecules undergo much higher scattering efficiencies when adsorbed on metal colloidal nanoparticles or rough metal surfaces. The SERS effect was discovered in 1974 by Fleischmann et al. [9]. The group discovered an anomalously large enhancement of the Raman signal of pyridine in the presence of a roughened silver electrode. The enhancement was initially attributed to greater than expected, or fractal-like, surface area, but subsequent reports showed that the anomalous intensity could not be accounted for by increased surface area and was, in fact, a new phenomenon, giving rise to the idea of the SERS cross-section [10, 11]. However, while SERS has become a large and extremely active field of study, there is still a debate on the exact details of its mechanism and its magnitude [12, 13].

Since then, several enhancement mechanisms were proposed in the early days of SERS. However, only two mechanisms are now broadly accepted, i.e., electromagnetic (EM) theory and chemical enhancement (CE) theory [8, 14, 15]. The electromagnetic models treat the molecule as a point dipole which responds to the enhanced local fields at or near the metal surface [16]. These enhanced fields, in turn, arise from roughness features that couple the incident field to surface plasmons [17]. On the other hand, chemical models attribute SERS intensity to modification of the molecular polarizability by interaction with the metal with ensuing molecular resonances, giving rise to enhancements such as those associated with resonance Raman scattering [18]. CE theory depends on the chemical interaction between probe molecules and the noble metal and is said to contribute only a maximum of about two to three orders of magnitude [19]. Both of these enhancements work simultaneously but are yet to be fully understood because of the difficulties in investigating the enhancements separately. Considering that the Raman signal is proportional to the square of dipole moment, $(P = \alpha E)$, both enhancement mechanism influences can be viewed as one changes the local electric field (E), and the second changes polarizability (α) near the analyzed molecule. Another way to understand the enhancement of SERS is by looking at the SERS intensity components [20].

$$I_{sers} = I_e N_{sur} \Omega A_e(\omega_e) A_s(\omega_s) \frac{d\sigma}{d\Omega}, \tag{10}$$

where $A_e(\omega_e)$ and $A_s(\omega_s)$ are electromagnetic surface-averaged intensity enhancement factors, I_e excitation light intensity, N_{sur} the number of adsorbed molecules excited by the light, and $\frac{d\sigma}{d\Omega}$ the solid angle of collection optics.

From Eq. (10), it follows that the Raman intensity can be enhanced in three ways:

i. by increasing the number of molecules that are on the metal surface compared to the smooth surface;

ii. by increasing the Raman cross section; and

iii. by increasing the electromagnetic surface averaged intensity enhancement factors.

Experiments have proved that by increasing the surface roughness, the number of absorbed molecules was changed only a few times, leaving us with the last two possibilities. They are electromagnetic (EM) and chemical contributions to the enhancement of Raman signal.

2.1 Chemical enhancement mechanism

CE requires the probe to be chemically bound to the SERS substrate. The CE can be grouped into three contributions to the chemical mechanism: (i) a resonance Raman (RR) effect due to the incident light matching an electronic transition in the molecule (10^3–10^6 contribution), (ii) a charge-transfer (CT) effect where the incident light is in resonance with a metal-molecule or molecule-metal transition. (10–10^4 contribution), (iii) a nonresonant chemical (CHEM) effect due to ground-state orbital overlap between the molecule and the metal (≤10–100 contribution) [21].

RR is a molecular resonance mechanism that arises from the incident light being resonant with a molecule, and without a metal surface, this leads to resonance

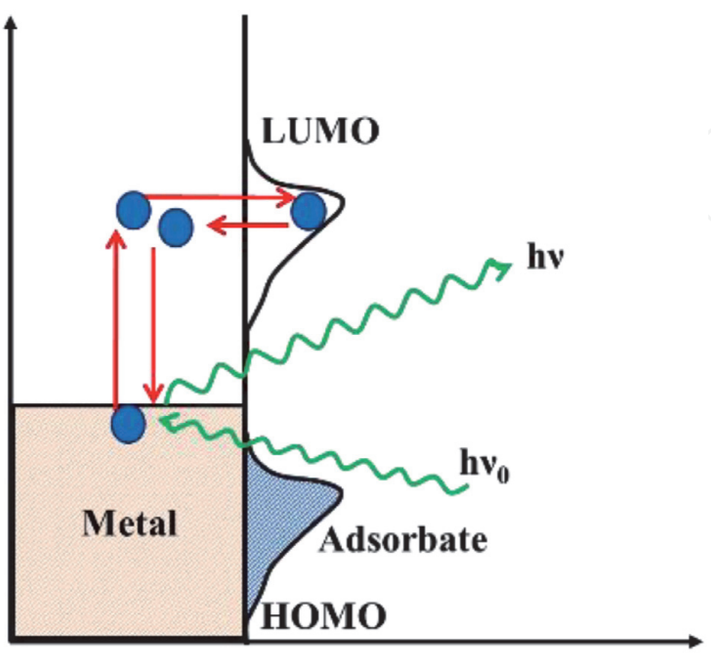

Figure 2.
Schematic diagram of the four-step process of the photon-driven charge transfer model for a molecule adsorbed on an electrode.

Raman scattering. RR involves the formation of a surface complex involving the metal and the analyte, leading to a change in the properties of the molecule (such as the possibility of resonance Raman scattering). The RR effect is typically thought of as a molecular property, and it has been included as a SERS mechanism since the presence of the metal surface can alter where this resonance lies. The CT effect only appears when the molecule and metal are close enough to allow for a sufficient overlap of their wave functions. In this mechanism, tunneling of electrons between the metal and adsorbate molecules takes place. Due to the transfer of an electron from metal to molecule or from molecule to metal, a negative ion is formed. Enhancement occurs when the energy of the negative ion is resonant with the incident photon. This mechanism is explained by considering the molecule and metal system as a whole. It is considered that the Fermi level of the metal layer lies between the molecular ground level and one or more excited states of the molecule. The charge transfer mechanism is short-ranged (0.1–0.5 nm) and strongly dependent on the geometry, bonding, and the molecule energy level [22]. The CHEM effect is the least studied and most difficult to quantify experimentally due to its small contribution to the overall enhancement. The formation of metal-molecular complexes mainly causes the CHEM effect due to chemical bonding [23]. This modifies the ability of the dipole to radiate energy, i.e., it can effectively oppose or amplify the dipole amplitude (**Figure 2**).

2.2 Electromagnetic mechanism

In theory, EM enhancement is analyte independent, while CE is probe-dependent and requires some chemical interaction to the metal surface [24]. Most of SERS enhancements are due to the EM enhancement mechanism and are a direct consequence of the roughness present on the noble metal surfaces [25]. The nanostructure can be formed on the substrate itself or by depositing noble metal nanoparticles. These metal nanoparticles can interact with the excitation light because of unique properties caused by their low dimensions (10–100 nm). The small size of the metal nanoparticles makes a special kind of light-induced electric polarization possible for their surface electrons. Collective oscillations of these electrons, driven by the alternating electric field of the light wave, are called surface plasma oscillations. At a particular frequency, plasmon oscillations are resonant with light; then electric field intensity and Raman scattering from the molecules attached to the nanostructures are enhanced [8, 26]. A locally strong light-induced electric field of plasmons in metal nanoparticle causes the increase of $A_e(\omega_e)$ and $A_s(\omega_s)$ factors. It is because nanoparticles work as a kind of optical antenna, redistributing and concentrating light energy near a nanoparticle. As a result, the cross-section of the light scattering processes, including Raman scattering, can be much larger than the geometrical cross-section of the metal nanoparticle.

The surface electron oscillations in metal nanoparticles can be derived from the classical Drude model, describing metal as a lattice of ions immersed into the "gas" consisting of the free electrons [27, 28]. In a static electric field, the internal field of the metals, generated by the displacement of free electrons, shield the external electric field. As a result, the external electrostatic field cannot create the electric field inside the metal. As a result, if electrostatic fields are applied to the metals, their dielectric permittivity is ambiguous. The dielectric permittivity is the measure of how much the electric field inside a material differs from that of a vacuum. However, when a high-frequency electric field is applied, the free electrons inside the metal cannot completely follow in time with the high-frequency oscillations of the electric field. It creates a situation where at very high frequencies, metal can pass the electric field from the incident light, i.e., behave as a dielectric. The high

transparency of these metals in the ultraviolet region can be explained by the fact that they have a lot of free electrons. Electrons of such metals as Al, Cu, Au, and Ag are not completely free but partially bounded.

The surface plasmon frequency ω_{sp} in small spherical metal nanoparticle includes the frequency of the volume plasma ω_p and permittivity of the surrounding dielectric [29]:

$$\omega_{sp} = \frac{\omega_p}{(1 + 2\varepsilon_d)^{\frac{1}{2}}} \tag{11}$$

Hence at the resonant frequency $\omega_{sp} = \omega$, from Eqs. (11) and (12),

$$\varepsilon_m = -2\varepsilon_d \tag{12}$$

From Eq. (12), it follows that the permittivity of metal should have a negative value. Few metals such as Cu, Ag, and Au exhibit strong visible light plasmon resonance, whereas other transition metals show only broadband in the ultraviolet region. Ag, in particular, is suitable for SERS applications in the visible and near IR because it has a tiny imaginary component in this region and thus is less "lossy" than other metals [30].

When monochromatic radiation of frequency ν_0 and electric filed E interacts with a molecule, it induces a Raman dipole oscillating at a frequency $\mu = \alpha E$. The oscillating Raman dipole radiates a power proportional to $|\mu|^2$ at frequency ν and is the frequency detected as Raman signal in far-field. The same phenomenological description can be applied to SERS. However, the presence of nanostructured metal surface alters the effects in the following ways [31–35]:

a. The electromagnetic field at the metallic surface can be dramatically increased and may result in a possible *local field enhancement*.

b. The radiation properties of the Raman dipole, μ, are affected by the metallic environment and may result in a possible *radiation enhancement*.

3. Applications of Raman spectroscopy

Raman spectrum can give rich information of analyte molecules, and SERS due to its higher signal intensity make it possible to detect analyte molecules in very low concentration, which enhances its practical applications [21]. This technique has a large number of applications in various fields, including trace chemical detection [21, 36], such as dye molecules [37–39], food additives [40, 41], pesticide trace detection [42–44], bioanalysis [45–49], and explosive detection [50, 51]. The detection of a trace amount of hazardous chemicals is also in high demand because of the increasing threat from toxic environments and unreliable food safety [52]. Melamine is a chemical compound and has been widely used in milk and pet food as an additive to increase protein percentage. However, since 2007, melamine, with its contaminant cyanuric acid, has become prominent because of the milk scandal. As a facile and simple spectroscopy technique, SERS has been used to detect melamine content [53, 54]. Apart from this, SERS has been widely used for bioanalysis, i.e., in the detection of biomolecules [55], cancer diagnosis [56, 57], urine component detection [58, 59], and in vivo molecular probing in live cells [60, 61], which play an important role in the life science for health care or treatment. Biomolecules, such as DNA, can also be detected using SERS [62, 63].

3.1 Raman spectroscopy for transition metal dichalcogenides (TMDs)

Transition metal dichalcogenides, as the names suggest, are a class of material that is made up of the transition metals (M = Mo, W, Ta, Pt) and chalcogenides (X = S, Se, Te). The unit cell of bulk MX_2 consists of X–M–X units, where one M plane is sandwiched between two X planes. Depending upon how these units are stacked, different kinds of polytypes are formed, for example:

1. 1T (one X–M–X unit in the unit cell, octahedral coordination, tetragonal symmetry, T stands for trigonal)

2. 2H (two X–M–X layers per repeat unit, trigonal prismatic coordination, hexagonal symmetry, H stands for hexagonal)

3. 3R (three X–M–X layers per repeat unit, trigonal prismatic coordination, rhombohedral symmetry, R stands for rhombohedral)

The schematic diagram of these polytypes is given in **Figure 3**.

In recent years, Raman spectroscopy is adopted to address the challenges in the characterization of these TMDs due to: (1) Many possible structures (generally the

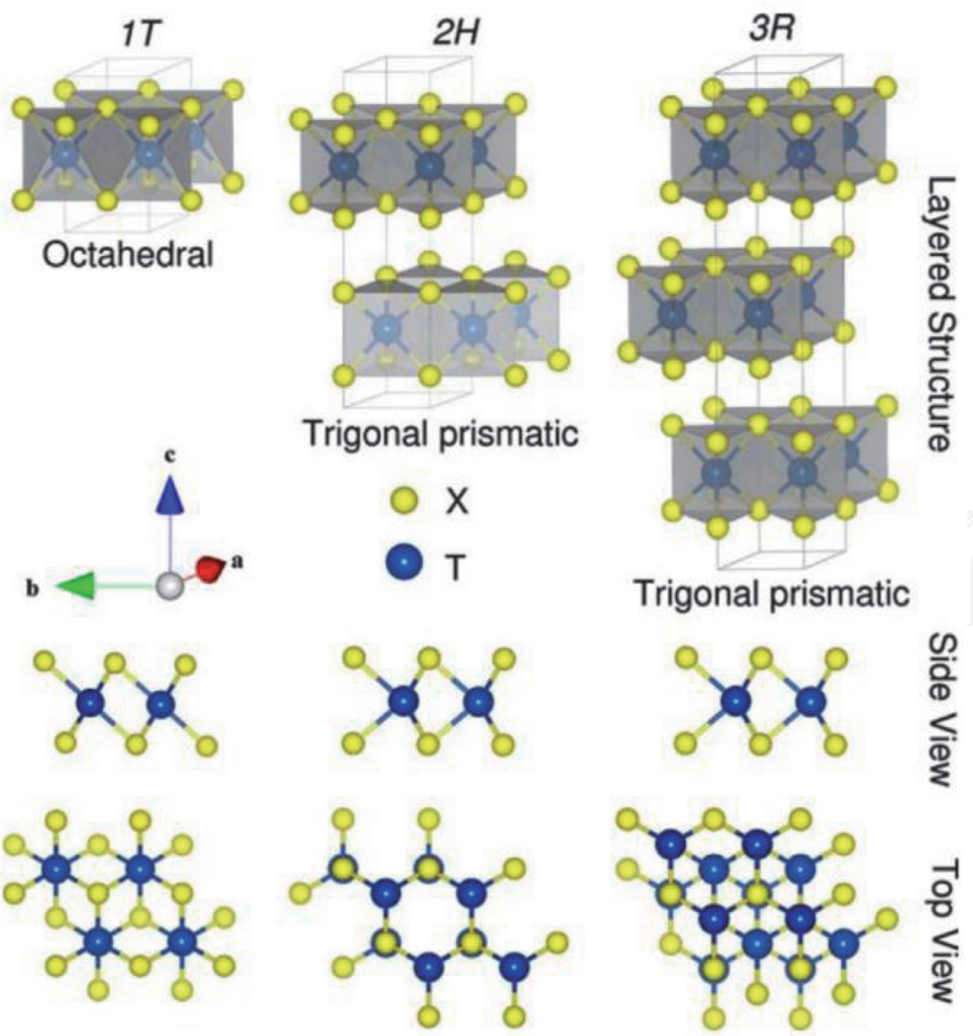

Figure 3.
Structural representation of 1T, 2H, and 3R TMC polytypes and their corresponding metal atom coordination. The side and top view of layered forms are shown [61].

stacking of layers has a rotational (or translational) freedom with reference to an axis perpendicular to (or also along) a 2D plane, giving them non-uniqueness); (2) weak interlayer interaction, which is much smaller than the intralayer interactions; and (3) observation of inner layers (the physical properties of each layer within the stacked TMDs are not selectively accessible except for the outermost layer). Other than resolving these challenges, Raman spectroscopy can identify functional groups, structural damage, unwanted by-products, and chemical modifications introduced during synthesis, processing, or its placement on the various substrates during device fabrication. It is spectroscopy, which is nondestructive, quick, and noninvasive for characterizing the TMD materials with high selectivity [64–66].

In general, the Raman spectroscopy has been widely used to determine the layers of the TMDs. For all the layered materials, which also includes TMDs, there are typically two categories of Raman vibrations. One is intralayer vibrations, which occur within a layer and normally appear in the high-frequency region of the spectra. The second category of Raman vibrations is observed due to the relative motion of the layers. These vibrations give the interlayer Raman modes, which are normally observed in the low-frequency region of the spectra ($<100\ cm^{-1}$).

In the layered TMDs, to determine the number of layers N for few-layer TMDs, high-frequency intralayer Raman modes can be used [67, 68]. For example, the layer number (N) dependence of the peak position and width for E^1_{2g} and A_{1g} of NL-MoS_2 is shown in **Figure 4(a)**. The A1g and E^1_{2g} modes undergo blue and redshifts with increasing numbers of layers for MoS_2.

The position of (E^1_{2g}) and (A_{1g}) with decreasing thickness from the bulk to 1 L shows opposite trends, as shown in **Figure 4(b)**.

However, these two modes would decrease in frequency from 2L to 1L based on the linear chain model (only van der Waals interactions are included). This unexpected behavior of E^1_{2g} suggests that interactions other than van der Waals forces also exist [68–70], which is also disclosed by the anomalous Davydov splitting between E^1_{2g} and E_{1u} [71].

Molina-Sanchez et al. [72] carefully examined and reported the relationship between the number of monolayers and the Raman active modes (A_{1g} and E^1_{2g}). They demonstrated that the weak interlayer interaction is the leading cause of the frequency increase (i.e., for A_{1g}) with the number of layers. Moreover, the decrease

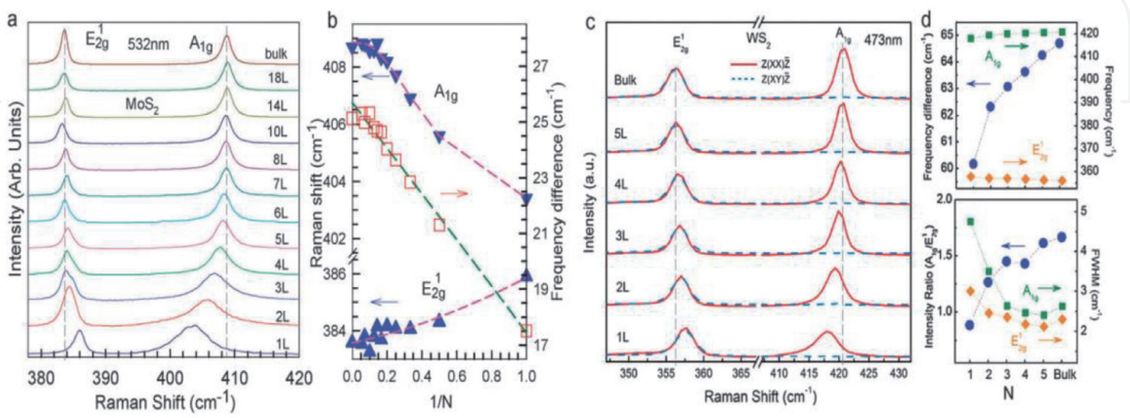

Figure 4.
(a) Raman spectra of NL-(N = 1–8, 10, 14 and 18) and bulk MoS_2. The two gray-dashed lines indicate Pos (E^1_{2g} E1 2g) and Pos(A_{1g}) in bulk MoS_2. (b) Frequency (ω) of E^1_{2g} and A_{1g} and the frequency difference ($\Delta\omega$) between E^1_{2g} and A_{1g} as a function of 1/N. For $1 \le N \le 5$, the linear fitting gives $\Delta\omega(A–E) = 25.8–8.4/N$. (c) Polarized Raman spectra of 1–5L and bulk WS_2, with the frequencies of E^1_{2g} and A_{1g} frequency difference, I (A_{1g})/I(E^1_{2g}), and peak width summarized in (d) [66, 73].

in the E^1_{2g} phonon frequency is associated with a stronger dielectric screening of the long-range Coulomb interaction (which is induced by the effective charges resulting from the relative displacement between Mo and S atoms) in a few layers and in bulk. Thus, it is expected to exhibit an anomalous frequency trend in which the A_{1g} mode increases in frequency with an increasing number of layers, while the E^1_{2g} mode decreases.

In the case of the WS_2, the proximity of the 2LA(M) and E^1_{2g} peaks makes it challenging to measure the accurate difference between the A_{1g} and E^1_{2g} peaks and increases the chance of error in determining the frequency shift of both the modes. To resolve this problem, Berkdemir et al. [74] reported a new method based on the ratio of the intensities of I_{2LA} and I_{A1g} peaks. In this method, the authors reported that the absolute intensity of the 2LA(M) mode increases with decreasing the number of layers, while the intensity of the A_{1g} displays the opposite behavior [74]. The behavior of the A_{1g} mode with a decreasing number of layers presumably results from weaker interlayer contributions to the phonon restoring forces.

3.2 Application of Raman spectroscopy in photovoltaics

Conducting polymers are widely used in organic light-emitting diodes, heterojunction diodes, organic thin-film transistors, solar cells, actuators, sensors, etc. [75–79]. Poly(3,4-ethylenedioxythiophene)-poly(styrene sulfonate) (PEDOT:PSS) is extensively used conducting polymer because of its high conductivity, excellent thermal stability, transparency, structural stability. PEDOT:PSS polymer is a promising candidate as a transparent electrode for optoelectronic devices. The solvent treatment of PEDOT:PSS films may affect the conformation of the polymer. The structure of the PEDOT chain changes from benzoid to quinoid structure after solvent treatment [75, 80]. The effect of the conformation of the PEDOT chains in the PEDOT:PSS film before and after the dimethyl sulfoxide (DMSO) treatment was studied by Raman spectroscopy. **Figure 5** shows the Raman spectra of PEDOT:PSS with different concentrations of DMSO. The most obvious change was observed for the strongest band between 1400 and 1500 cm^{-1}. The highly

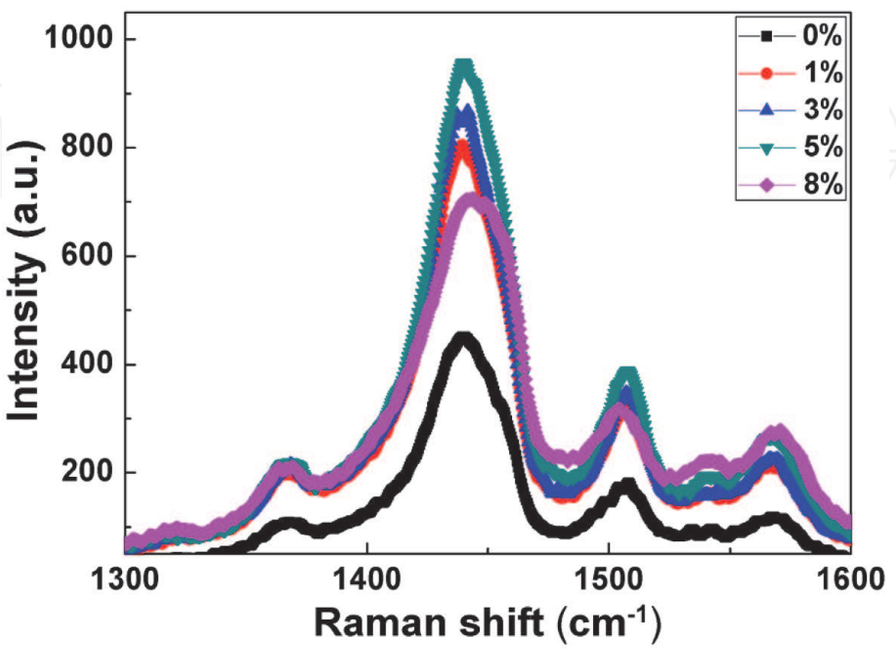

Figure 5.
Raman spectra of PEDOT:PSS films with 0–8 vol.% DMSO.

conductive PEDOT:PSS film exhibits a narrower band. This change is similar to that of PEDOT:PSS film treated with ethylene glycols reported by Xia et al. [81]. These vibrational modes correspond to the stretching vibrations of $C_\alpha = C_\beta$ on the five-member ring of PEDOT.

The band at 1440 cm^{-1} is associated with the $C_\alpha{=}C_\beta$ symmetric vibration. The band near about 1368 cm^{-1} is associated with the $C_\beta{-}C_\beta$ stretching. Raman peaks located at 1508 and 1568 cm^{-1} are associated with the $C_\alpha{=}C_\beta$ asymmetric stretching vibrations. The band at 1540 cm^{-1} has been related to the splitting of these asymmetrical stretching vibrations [79, 81–84]. Two kinds of resonant structures have been proposed for PEDOT, namely, benzoid and quinoid structure. For coil conformation, benzoid structure is the favorite structure, and quinoid structure is the favorite structure for linear and expanded-coil structure. Both benzoid and quinoid resonant structures exist simultaneously in pristine PEDOT:PSS film. The benzoid structure may be transformed into the quinoid structure after DMSO treatment so that quinoid structure becomes dominant in the highly conductive PEDOT:PSS film. The conducting PEDOT:PSS films are vastly used in optoelectronic devices.

4. SERS substrates

"SERS substrates" are any nanostructured metallic platform that supports plasmon resonance and amplifies Raman signals [85]. Herein, SERS substrates are classified into two broad distinctions:

a. **Random morphology SERS substrates** include roughened electrodes, metallic silver and gold colloids, metal-island film on planer substrate, and other related substrates.

b. **Ordered or periodic metallic SERS substrates** include arrays of regular morphology metallic nanotextures created on planar substrates using nanolithography and other physical vapor deposition techniques.

4.1 Random morphology SERS substrates

Random morphology SERS substrates are inhomogeneous and are not highly reproducible [86]. Roughened electrodes are the most primitive SERS substrate and were discovered by Fleischmann et al. [9]. These substrates are typically created by running the redox cycle in an electrochemical cell containing a metallic salt solution. Such substrates have gained popularity due to an ability to adjust electrode potential to understand the charge transfer phenomenon between adsorbate and metallic surface [87]. Regardless, the importance of this substrate is decreasing substantially due to relatively low enhancement factors.

Among the random morphology SERS substrates, silver or gold colloids are the most common substrates used in both early and more recent studies. Since colloids are easy to produce in a laboratory and tend to generate large enhancement factors, most researchers are still involved in colloid-based SERS rather than more sophisticated substrates [88, 89]. Metallic colloids are also of historic significance related to SERS development, as the first single-molecule SERS detection was reported using colloid substrates [90]. In colloid-based methods, nanoparticle size and geometry can be controlled by altering experimental conditions. One of the most popular methods for controlling nanoparticle morphology stems from the polyol synthesis of silver nanocubes by Sun and Xia [78]. In addition to the nanocubes, various groups have produced octahedra and cuboctahedra [91] and octapods [92].

El-Sayed et al. have contributed to the control of particle morphology, yielding a variety of interesting and useful structures [93–95]. Since the size, shape, and material of the particles govern the resulting plasmonic resonance characteristics, significant effort has been exerted in the control of plasmon resonance via core-shell and alloyed particles, to which the Halas group has a large contribution [96–98].

SERS substrates have also been fabricated by depositing nanoparticles onto different surfaces. These simple deposition approaches include micro pipetting [99], soaking [100], screen-printing [101], filtration [102], and inkjet printing [103]. However, a major concern with these simple deposition processes is that the hotspots are generated and distributed randomly over the substrate. The differences in metallic particle sizes and their shapes due to the differences in preparation recipes can lead to several orders of magnitude difference in the SERS enhancement factor.

In order to obtain more consistent hotspots from nanoparticles, researchers have explored both self-assembly [99] and directed assembly techniques, such as the Langmuir-Blodgett techniques [91], to create regular arrays of nanoparticles. However, these techniques also introduce more complexity to the fabrication process.

4.2 Periodic or uniform SERS substrate

Although metallic colloidal particles are known for their high SERS EF and possibility to accomplish SERS spectra of a single molecule, it is often challenging to reproduce or routinely deliver such a high performing SERS feature. To overcome this issue, a few alternatives have been introduced on engineering periodic arrays of metallic nanostructured SERS substrates. Nanosphere lithography (NSL), developed by Van Duyne et al., is one of the most extensively used nano-fabrication procedures used in understanding SERS phenomena and performing plasmonic-based sensing [104–106]. It involves the assembly of polystyrene nanospheres into a regular array, using this as a mask to create periodic nanostructures, sometimes called “metal island films,” by the evaporation of Ag or Au through the gaps created by the packing of the nanospheres, followed by removal of the nanospheres. A variation on this method, called “metal film over nanospheres,” is to evaporate a metal film directly onto the nanosphere template, using closely-packed nanospheres to pattern the substrate surface itself [107]. Electron beam lithography (EBL) is another most widely used conventional nanofabrication technique in designing uniform and controlled morphology SERS substrates [108, 109]. In the literature, there are many SERS-active surface designs prepared with EBL [110, 111]. These designs are mainly periodic arrays of simple nano-structures, and generally, the relation between the LSP resonance wavelength and SERS signal enhancement is studied. For example, Le Ru et al. have taken SERS measurements, from periodic gold dot, square, and triangle arrays, from “Rhodamine 6G” [112]. They demonstrated that the localized plasmon resonances, which are at the origin of visible-NIR extinction spectra and the SERS effect, can be tuned to any desired wavelength by varying the particle shape/size and spacing, thus tuning the Raman amplification. In a very similar study, Gunnarsson et al. studied similar Ag structures on a silicon wafer for the same molecule and reported that better results are obtained than nano-roughened Ag film [110]. They investigated the size and geometry dependence of the SERS effect on supported particles, by manufacturing artificial structures by modern nanofabrication techniques. Arrays of 100–200 nm silver particles of different shapes were prepared on a Si wafer by electron beam lithography. Kahl et al. have shown that the SERS measurements of “Rhodamine 6G” on gold periodic nano-dot arrays and grating structures resulted in order of magnitude better SERS

enhancement when compared with metal-island film substrates [113]. They demonstrated two different methods of substrate fabrication by e-beam lithography. In the first method, regular fields of nanoparticles are produced by the lift-off technique. A silver layer is evaporated on the structured resist, and the resist is removed afterward. In the second method, gratings or crossed gratings are transferred into a silicon wafer with a thermal oxide surface layer by reactive ion etching (RIE). Then, the e-beam resist is removed, and finally, a silver layer is evaporated. Hatab et al. have demonstrated significant SERS enhancement factors exceeding 10^{11}, resulting from a new configuration of elevated gold bowtie nano-antenna arrays with optimized array periodicity [114]. A process combining nanofabrication steps of pattern definition by EBL, metal deposition, lift-off, and RIE arranged in a particular sequence was used to fabricate the elevated gold bowtie arrays on Si wafers. The elevated bowties allow the manifestation of intrinsic plasmonic coupling effects in suspended nanocavities, or the tip-to-tip nanogaps, from structures that are not in physical contact with a substrate. This configuration results in up to two orders of additional magnitude enhancement in SERS response compared to that of nonelevated bowtie arrays. The diversity of designs is endless when fabrication with EBL is considered. However, these techniques, while excellent at making SERS substrates with defined characteristics, are hampered by the slow, serial nature and high cost of the processes used in their fabrication.

4.3 SERS from silver columnar film

The SERS enhancement strongly depends on the substrate. As already discussed earlier, various techniques have been proposed and identified for the fabrication of the SERS substrate. However, only a few methods are available to develop uniform, reproducible, robust, stable, and cost-effective SERS substrates. Recently, silver columnar thin films fabricated by glancing angle deposition (GLAD) have been identified as high sensitivity SERS active substrates [115–122]. A remarkable SERS enhancement factor with applications in sensing the biomolecules at very low concentrations has been observed on the silver nanorod arrays [123]. To understand the SERS mechanism and attain a maximum possible enhancement, large numbers of studies have been performed on the Ag nanorod (AgNR) arrays. In an interesting study, Chaney et al. have investigated the SERS response as a function of the nanorod length using trans-1,2-bis(4-pyridyl)ethane (BPE) as a probe molecule at an excitation wavelength of 785 nm [124]. They found that the SERS intensity increases dramatically with nanorod length. Zhou et al. fabricated aligned, single-crystalline AgNRs on planar Si substrates by GLAD technique, with sample substrate cooled by liquid nitrogen in the e-beam deposition system [125]. They were successful in detecting aqueous solution of10^{-12} molL^{-1} Rhodamine 6G by the porous Ag film with nanorods. They also deposited AgNRs on Ag, Al, Si, and Ti thin films with a thickness of 100 and 400 nm, respectively, to achieve layers with different reflectivities. The SERS intensity of the AgNRs grown on Ag thin film was found to be higher than others, and the SERS intensity of the AgNRs on Al film was larger than that on Ti film, and the AgNRs on Si film showed the minimum SERS intensity. They concluded that the larger the under-layer reflectivity, the larger the SERS performance of substrate. So, the pre-deposition of Ag layer under AgNRs can be an effective way to promote the SERS performance of AgNRs. Zhang et al. have made AgNRs in film grow into periodic patterns at a micro-nano scale, and they showed that the AgNR film with periodic patterns exhibits better SERS performance than Ag film with nanorods arranged randomly as before [126]. He et al. also reported a new scalable strategy based on dynamic shadowing growth (DSG) to fabricate large-scale chiral Swiss roll nanostructures. They developed a chiral

conical Swiss roll nanostructure by helically stacking Ag films on a SiO_2 frustum with SiO_2 films as insulating layers [127]. They also showed that the chiral dichroism (CD) spectral feature can be tuned by changing the bead diameter. They achieved a broadband CD response in visible to near-IR region by making the bead diameter a few hundred nanometers. Mark et al. combined the low-temperature shadow deposition with nanoscale patterning to fabricate nanocolloids with anisotropic three-dimensional shapes, feature sizes down to 20 nm [128]. They first deposited a uniform hexagonal array of Au nanodots deposited onto a Si wafer by micellar nanolithography. Then they deposited material onto the substrate by physical vapor deposition at grazing incidence. To reduce the adatoms' mobility and reduce the diffuse during growth, they cooled the substrate. So, by combining the uniform nano-seeding and low-temperature growth, they fabricated various complex hybrid nanostructures of many materials like from Al_2O_3, Ti, and Cu. GLAD has also emerged as a powerful tool for the fabrication of 3D chiral plasmonic nanostructures. Titus et al. investigated the optical properties of Ti-doped Ag helices in the visible and near-infrared ranges using transmission ellipsometry and spectroscopy fabricated by GLAD [129]. Nair et al. reported the fabrication of wafer-scale 3D chiral nanoplasmonic substrates with different dielectric templates, namely, silica, magnesium fluoride, and titanium dioxide using GLAD [130]. They have also investigated the effect of interparticle separation on the chiroptical response of chiral nanohelices [131].

Hence, we can see that the development of fabrication and application of substrates for SERS is driven by nanotechnology and the development of high-end fabrication processes. Increasingly SERS substrates with high sensitivity and reproducibility are invented by electrochemical deposition, physical vapor deposition of the metal film, metal nanoparticle colloids, and so forth and applied into various fields, such as detection of pollutants at trace level, surface analysis, biomolecule, and bacteria detection. With the development of SERS substrate, advancement in Raman spectrometers, and tip-enhanced Raman scattering (as the combination of SERS and atomic force microscopy), SERS is becoming increasingly popular as a detection and diagnostic tool.

DOI: http://dx.doi.org/10.5772/intechopen.92614

Author details

Samir Kumar[1*], Prabhat Kumar[2], Anamika Das[3] and Chandra Shakher Pathak[4]

1 Department of Micro Engineering, Graduate School of Engineering, Kyoto University, Kyoto, Japan

2 Department of Thin Films and Nanostructures, Institute of Physics of the Czech Academy of Sciences, Prague, Czech Republic

3 Department of Paramedical Sciences, Guru Kashi University, Bhatinda, India

4 Department of Solar Energy and Environmental Physics, Ben-Gurion National Solar Energy Center, Jacob Blaustein Institutes for Desert Research, Ben-Gurion University of the Negev, Midreshet Ben-Gurion, Israel

*Address all correspondence to: drsamirkumar2017@gmail.coom

References

[1] Weber WH, Merlin R. Raman Scattering in Materials Science. Berlin, Heidelberg: Springer; 2000

[2] Smekal A. Zur Quantentheorie der Dispersion. Die Naturwissenschaften. 1923;**11**:873-875. DOI: 10.1007/BF01576902

[3] Krishnan KS, Raman CV. A new class of spectra due to secundary radiation. Indian Journal of Physics. 1928;**2**: 399-419

[4] Krishnan RS, Shankar RK. Raman effect: History of the discovery. Journal of Raman Specroscopy. 1981;**10**:1-8. DOI: 10.1002/jrs.1250100103

[5] Schrader B. Infrared and Raman Spectroscopy: Methods and Applications. Weinheim (Federal Republic of Germany): VCH; 1995

[6] Long DA. Quantum mechanical theory of Rayleigh and Raman scattering. In: Long DA, editor. The Ram Effect. Chichester, UK: John Wiley & Sons, Ltd.; 2002. pp. 49-84. DOI: 10.1002/0470845767.ch4

[7] Smith E, Dent G. Introduction, basic theory and principles. In: Smith E, Dent G, editors. Modern Raman Spectrosopy—A Practical Approach. Vol. 5. 2005. pp. 1-21. DOI: 10.1002/0470011831.ch1

[8] Moskovits M. Surface-enhanced spectroscopy. Reviews of Modern Physics. 1985;**57**:783-826. DOI: 10.1103/RevModPhys.57.783

[9] Fleischmann M, Hendra PJ, McQuillan AJ. Raman spectra of pyridine adsorbed at a silver electrode. Chemical Physics Letters. 1974;**26**: 163-166. DOI: 10.1016/0009-2614(74)85388-1

[10] Jeanmaire DL, Van Duyne RP. Surface Raman spectroelectrochemistry. Part I. Heterocyclic, aromatic, and aliphatic amines adsorbed on the anodized silver electrode. Journal of Electroanalytical Chemistry. 1977;**84**: 1-20. DOI: 10.1016/S0022-0728(77)80224-6

[11] Albrecht MG, Creighton JA. Intense Raman spectra at a roughened silver electrode. Electrochimica Acta. 1978;**23**: 1103-1105. DOI: 10.1016/0013-4686(78)85022-1

[12] Le Ru EC, Etchegoin PG. Quantifying SERS enhancements. MRS Bulletin. 2013;**38**:631-640. DOI: 10.1557/mrs.2013.158

[13] Bochenkov V, Baumberg J, Noginov M, Benz F, Aldewachi H, Schmid S, et al. Applications of plasmonics: General discussion. Faraday Discussions. 2015;**178**:435-466. DOI: 10.1039/C5FD90025E

[14] Kneipp K, Moskovits M, Kneipp H. Surface-Enhanced Raman Scattering: Physics and Applications. Berlin, Heidelberg: Springer; 2006

[15] Le Ru EC, Etchegoin PG, Meyer M. Enhancement factor distribution around a single surface-enhanced Raman scattering hot spot and its relation to single molecule detection. The Journal of Chemical Physics. 2006;**125**:204701. DOI: 10.1063/1.2390694

[16] Nardou E, Vouagner D, Jurdyc AM, Berthelot A, Pillonnet A, Sablonire V, et al. Distance dependence of the surface enhanced Raman scattering effect observed in amorphous TiO_2 on nanostructured gold. Optical Materials. 2011;**33**:1907-1910. DOI: 10.1016/j.optmat.2011.03.024

[17] Zhao Y, Liu X, Lei DY, Chai Y. Effects of surface roughness of Ag thin films on surface-enhanced Raman

spectroscopy of graphene: Spatial nonlocality and physisorption strain. Nanoscale. 2014;**6**:1311-1317. DOI: 10.1039/c3nr05303b

[18] McNay G, Eustace D, Smith WE, Faulds K, Graham D. Surface-enhanced Raman scattering (SERS) and surface-enhanced resonance Raman scattering (SERRS): A review of applications. Applied Spectroscopy. 2011;**65**:825-837. DOI: 10.1366/11-06365

[19] Su J-P, Lee Y-T, Lu S-Y, Lin JS. Chemical mechanism of surface-enhanced Raman scattering spectrum of pyridine adsorbed on Ag cluster: *Ab initio* molecular dynamics approach. Journal of Computational Chemistry. 2013;**34**:2806-2815. DOI: 10.1002/jcc.23464

[20] Kruszewski S. Enhancement mechanisms in the SERS phenomenon. In: Proceedings SPIE 3320, Tenth Polish-Czech-Slovak Optical Conference: Wave and Quantum Aspects of Contemporary Optics. 1 January 1998. DOI: 10.1117/12.301353

[21] Schlücker S. Surface-enhanced Raman spectroscopy: Concepts and chemical applications. Angewandte Chemie, International Edition. 2014;**53**: 4756-4795. DOI: 10.1002/anie.201205748

[22] Ueba H, Ichimura S, Yamada H. Where are we in the study of SERS? Role of chemisorption and charge transfer. Surface Science. 1982;**119**:433-448. DOI: 10.1016/0039-6028(82)90309-0

[23] Saikin SK, Olivares-Amaya R, Rappoport D, Stopa M, Aspuru-Guzik A. On the chemical bonding effects in the Raman response: Benzenethiol adsorbed on silver clusters. Physical Chemistry Chemical Physics. 2009;**11**: 9401-9411. DOI: 10.1039/b906885f

[24] Otto A, Mrozek I, Grabhorn H, Akemann W. Surface-enhanced Raman scattering. Journal of Physics. Condensed Matter. 1992;**4**:1143-1212. DOI: 10.1088/0953-8984/4/5/001

[25] Saikin SK, Chu Y, Rappoport D, Crozier KB, Aspuru-Guzik A. Separation of electromagnetic and chemical contributions to surface-enhanced Raman spectra on nanoengineered plasmonic substrates. Journal of Physical Chemistry Letters. 2010;**1**:2740-2746. DOI: 10.1021/jz1008714

[26] Kneipp K. Surface-enhanced Raman scattering. Physics Today. 2007;**60**: 40-46. DOI: 10.1063/1.2812122

[27] Dressel M, Scheffler M. Verifying the Drude response. Annalen der Physik. 2006;**15**:535-544. DOI: 10.1002/andp.200510198

[28] Mahmudin L, Suharyadi E, Bambang A, Utomo S, Abraha K. Optical properties of silver nanoparticles for surface plasmon resonance (SPR)-based biosensor applications. Journal of Modern Physics. 2015;**6**:1071-1076. DOI: 10.4236/jmp.2015.68111

[29] Gordon R. Surface plasmon nanophotonics: A tutorial. IEEE Nanotechnology Magazine. 2008;**2**: 12-18. DOI: 10.1109/MNANO.2008.931481

[30] Alsawafta M, Wahbeh M, Van Truong V. Plasmonic modes and optical properties of gold and silver ellipsoidal nanoparticles by the discrete dipole approximation. Journal of Nanomaterials. 2012;**2012**. DOI: 10.1155/2012/457968

[31] Deng CY, Zhang GL, Zou B, Shi HL, Liang YJ, Li YC, et al. Local electric field enhancement of neighboring Ag nanoparticles in surface enhanced Raman scattering. Advances in Materials Research. 2013;**760–762**: 801-805. DOI: 10.4028/www.scientific.net/AMR.760-762.801

[32] Hexter RM, Albrecht MG. Metal surface Raman spectroscopy: Theory. Spectrochimica Acta Part A: Molecular Spectroscopy. 1979;**35**:233-251. DOI: 10.1016/0584-8539(79)80143-9

[33] Cialla D, Petschulat J, Hübner U, Schneidewind H, Zeisberger M, Mattheis R, et al. Investigation on the second part of the electromagnetic SERS enhancement and resulting fabrication strategies of anisotropic plasmonic arrays. ChemPhysChem. 2010;**11**: 1918-1924. DOI: 10.1002/cphc.200901009

[34] Gersten JI, Nitzan A. Electromagnetic theory: A spheroidal model. In: Chang RK, Furtak TE, editors. Surface Enhanced Raman Scattering. Boston, MA, US: Springer; 1982. pp. 89-107. DOI: 10.1007/978-1-4615-9257-0_5

[35] Zeman EJ, Schatz GC. An accurate electromagnetic theory study of surface enhancement factors for silver, gold, copper, lithium, sodium, aluminum, gallium, indium, zinc, and cadmium. The Journal of Physical Chemistry. 1987; **91**:634-643. DOI: 10.1021/j100287a028

[36] Zhang L, Xu J, Mi L, Gong H, Jiang S, Yu Q. Multifunctional magnetic-plasmonic nanoparticles for fast concentration and sensitive detection of bacteria using SERS. Biosensors & Bioelectronics. 2012;**31**: 130-136. DOI: 10.1016/j.bios.2011.10.006

[37] Zhao X, Zhang B, Ai K, Zhang G, Cao L, Liu X, et al. Monitoring catalytic degradation of dye molecules on silver-coated ZnO nanowire arrays by surface-enhanced Raman spectroscopy. Journal of Materials Chemistry. 2009;**19**: 5547-5553. DOI: 10.1039/B902883H

[38] Prikhodko SV, Rambaldi DC, King A, Burr E, Muros V, Kakoulli I. New advancements in SERS dye detection using interfaced SEM and Raman spectromicroscopy (μRS). Journal of Raman Specroscopy. 2015;**46**: 632-635. DOI: 10.1002/jrs.4710

[39] Kumar S, Lodhi DK, Singh JP. Highly sensitive multifunctional recyclable Ag-TiO_2 nanorod SERS substrates for photocatalytic degradation and detection of dye molecules. RSC Advances. 2016;**6**: 45120-45126. DOI: 10.1039/C6RA06163J

[40] Granger JH, Schlotter NE, Crawford AC, Porter MD. Prospects for point-of-care pathogen diagnostics using surface-enhanced Raman scattering (SERS). Chemical Society Reviews. 2016;**45**:3865-3882. DOI: 10.1039/C5CS00828J

[41] Craig AP, Franca AS, Irudayaraj J. Surface-enhanced Raman spectroscopy applied to food safety. Annual Review of Food Science and Technology. 2013;**4**: 369-380. DOI: 10.1146/annurev-food-022811-101227

[42] Wang P, Wu L, Lu Z, Li Q, Yin W, Ding F, et al. Gecko-inspired nanotentacle SERS substrate for rapid sampling and reliable detection of pesticide residues in fruits and vegetables. Analytical Chemistry. 2017; **89**:2424-2431. DOI: 10.1021/acs.analchem.6b04324

[43] Furini LN, Constantino CJL, Sanchez-Cortes S, Otero JC, López-Tocón I. Adsorption of carbendazim pesticide on plasmonic nanoparticles studied by surface-enhanced Raman scattering. Journal of Colloid and Interface Science. 2016;**465**:183-189. DOI: 10.1016/j.jcis.2015.11.045

[44] Kumar S, Goel P, Singh JP. Flexible and robust SERS active substrates for conformal rapid detection of pesticide residues from fruits. Sensors and Actuators B: Chemical. 2017;**241**: 577-583. DOI: 10.1016/j.snb.2016.10.106

[45] Jarvis RM, Goodacre R. Discrimination of bacteria using surface-enhanced Raman spectroscopy. Analytical Chemistry. 2004;**76**:40-47. DOI: 10.1021/ac034689c

[46] Wu X, Huang YW, Park B, Tripp RA, Zhao Y. Differentiation and classification of bacteria using vancomycin functionalized silver nanorods array based surface-enhanced Raman spectroscopy and chemometric analysis. Talanta. 2015; **139**:96-103. DOI: 10.1016/j.talanta.2015.02.045

[47] Xu K, Zhou R, Takei K, Hong M. Toward flexible surface-enhanced Raman scattering (SERS) sensors for point-of-care diagnostics. Advancement of Science. 2019;**6**:1900925. DOI: 10.1002/advs.201900925

[48] Kumar S, Lodhi DK, Goel P, Neeti N, Mishra P, Singh JP. A facile method for fabrication of buckled PDMS silver nanorod arrays as active 3D SERS cages for bacterial sensing. Chemical Communications. 2015;**51**: 12411-12414. DOI: 10.1039/C5CC03604F

[49] Kumar S, Namura K, Suzuki M. Proposal for a gel-based SERS sensor. Proceedings of SPIE. 2019;**10894**: 1089414. DOI: 10.1117/12.2506951

[50] Hakonen A, Andersson PO, Stenbæk Schmidt M, Rindzevicius T, Käll M. Explosive and chemical threat detection by surface-enhanced Raman scattering: A review. Analytica Chimica Acta. 2015;**893**:1-13. DOI: 10.1016/j.aca.2015.04.010

[51] Fierro-Mercado PM, Hernández-Rivera SP. Highly sensitive filter paper substrate for SERS trace explosives detection. International Journal of Spectroscopy. 2012;**716527**:7. Available from: http://www.hindawi.com/journals/ijs/2012/716527/

[52] Hakonen A, Wang F, Andersson PO, Wingfors H, Rindzevicius T, Schmidt MS, et al. Hand-held femtogram detection of hazardous picric acid with hydrophobic Ag nanopillar SERS substrates and mechanism of elasto-capillarity. ACS Sensors. 2017;**2**:198-202. DOI: 10.1021/acssensors.6b00749

[53] Giovannozzi AM, Rolle F, Sega M, Abete MC, Marchis D, Rossi AM. Rapid and sensitive detection of melamine in milk with gold nanoparticles by surface enhanced Raman scattering. Food Chemistry. 2014;**159**:250-256. DOI: 10.1016/j.foodchem.2014.03.013

[54] Du X, Chu H, Huang Y, Zhao Y. Qualitative and quantitative determination of melamine by surface-enhanced Raman spectroscopy using silver nanorod array substrates. Applied Spectroscopy. 2010;**64**:781-785

[55] Hughes J, Izake EL, Lott WB, Ayoko GA, Sillence M. Ultra sensitive label free surface enhanced Raman spectroscopy method for the detection of biomolecules. Talanta. 2014;**130**: 20-25. DOI: 10.1016/j.talanta.2014.06.012

[56] Kong KV, Leong WK, Lam Z, Gong T, Goh D, Lau WKO, et al. A rapid and label-free SERS detection method for biomarkers in clinical biofluids. Small. 2014;**10**:5030-5034. DOI: 10.1002/smll.201401713

[57] Zhu J, Zhou J, Guo J, Cai W, Liu B, Wang Z, et al. Surface-enhanced Raman spectroscopy investigation on human breast cancer cells. Chemistry Central Journal. 2013;**7**:37. DOI: 10.1186/1752-153X-7-37

[58] Dong R, Weng S, Yang L, Liu J. Detection and direct readout of drugs in human urine using dynamic surface-enhanced Raman spectroscopy and support vector machines. Analytical

Chemistry. 2015;**87**:2937-2944. DOI: 10.1021/acs.analchem.5b00137

[59] Villa JEL, Poppi RJ. A portable SERS method for the determination of uric acid using a paper-based substrate and multivariate curve resolution. The Analyst. 2016;**141**:1966-1972. DOI: 10.1039/c5an02398j

[60] Willets KA. Surface-enhanced Raman scattering (SERS) for probing internal cellular structure and dynamics. Analytical and Bioanalytical Chemistry. 2009;**394**:85-94. DOI: 10.1007/s00216-009-2682-3

[61] Radziuk D, Moehwald H. Prospects for plasmonic hot spots in single molecule SERS towards the chemical imaging of live cells. Physical Chemistry Chemical Physics. 2015;**17**:21072-21093. DOI: 10.1039/C4CP04946B

[62] Lim D-K, Jeon K-S, Hwang J-H, Kim H, Kwon S, Suh YD, et al. Highly uniform and reproducible surface-enhanced Raman scattering from DNA-tailorable nanoparticles with 1-nm interior gap. Nature Nanotechnology. 2011;**6**:452-460. DOI: 10.1038/nnano.2011.79

[63] Harper MM, McKeating KS, Faulds K. Recent developments and future directions in SERS for bioanalysis. Physical Chemistry Chemical Physics. 2013;**15**:5312-5328. DOI: 10.1039/c2cp43859c

[64] Zhang X, Tan QH, Bin Wu J, Shi W, Tan PH. Review on the Raman spectroscopy of different types of layered materials. Nanoscale. 2016;**8**:6435-6450. DOI: 10.1039/c5nr07205k

[65] Saito R, Tatsumi Y, Huang S, Ling X, Dresselhaus MS. Raman spectroscopy of transition metal dichalcogenides. Journal of Physics. Condensed Matter. 2016;**28**:353002. DOI: 10.1088/0953-8984/28/35/353002

[66] Zhang X, Qiao X-F, Shi W, Wu J-B, Jiang D-S, Tan P-H. Phonon and Raman scattering of two-dimensional transition metal dichalcogenides from monolayer, multilayer to bulk material. Chemical Society Reviews. 2015;**44**:2757-2785. DOI: 10.1039/C4CS00282B

[67] Li H, Zhang Q, Yap CCR, Tay BK, Edwin THT, Olivier A, et al. From bulk to monolayer MoS_2: Evolution of Raman scattering. Advanced Functional Materials. 2012;**22**:1385-1390. DOI: 10.1002/adfm.201102111

[68] Lee C, Yan H, Brus LE, Heinz TF, Hone J, Ryu S. Anomalous lattice vibrations of single- and few-layer MoS_2. ACS Nano. 2010;**4**:2695-2700. DOI: 10.1021/nn1003937

[69] Molina-Sánchez A, Wirtz L. Phonons in single-layer and few-layer MoS_2 and WS_2. Physical Review B. 2011;**84**:155413. DOI: 10.1103/PhysRevB.84.155413

[70] Luo X, Zhao Y, Zhang J, Xiong Q, Quek SY. Anomalous frequency trends in MoS_2 thin films attributed to surface effects. Physical Review B. 2013;**88**:075320. DOI: 10.1103/PhysRevB.88.075320

[71] Verble JL, Wieting TJ. Lattice mode degeneracy in MoS_2 and other layer compounds. Physical Review Letters. 1970;**25**:362-365. DOI: 10.1103/PhysRevLett.25.362

[72] Molina-Sánchez A, Wirtz L. Phonons in single-layer and few-layer MoS_2 and WS_2. Physical Review B: Condensed Matter and Materials Physics. 2011;**84**:1-8. DOI: 10.1103/PhysRevB.84.155413

[73] Zhao W, Ghorannevis Z, Amara KK, Pang JR, Toh M, Zhang X, et al. Lattice dynamics in mono- and few-layer sheets of WS_2 and WSe_2. Nanoscale. 2013;**5**:9677. DOI: 10.1039/c3nr03052k

[74] Berkdemir A, Gutiérrez HR, Botello-Méndez AR, Perea-López N, Elías AL, Chia C-I, et al. Identification of individual and few layers of WS_2 using Raman spectroscopy. Scientific Reports. 2013;**3**:1755. DOI: 10.1038/srep01755

[75] Pathak CS, Singh JP, Singh R. Effect of dimethyl sulfoxide on the electrical properties of PEDOT:PSS/n-Si heterojunction diodes. Current Applied Physics. 2015;**15**:528-534. DOI: 10.1016/j.cap.2015.01.020

[76] Pathak CS, Singh JP, Singh R. Modification of electrical properties of PEDOT:PSS/p-Si heterojunction diodes by doping with dimethyl sulfoxide. Chemical Physics Letters. 2016;**652**: 162-166. DOI: 10.1016/j.cplett.2016.04.029

[77] Palumbiny CM, Heller C, Schaffer CJ, Körstgens V, Santoro G, Roth SV, et al. Molecular reorientation and structural changes in cosolvent-treated highly conductive PEDOT:PSS electrodes for flexible indium tin oxide-free organic electronics. Journal of Physical Chemistry C. 2014; **118**:13598-13606. DOI: 10.1021/jp501540y

[78] Sun Y, Xia Y. Shape-controlled synthesis of gold and silver nanoparticles. Science. 2002;**298**(5601): 2176. DOI: 10.1126/science.1077229

[79] Sun K, Zhang S, Li P, Xia Y, Zhang X, Du D, et al. Review on application of PEDOTs and PEDOT:PSS in energy conversion and storage devices. Journal of Materials Science: Materials in Electronics. 2015;**26**: 4438-4462. DOI: 10.1007/s10854-015-2895-5

[80] He L, Jiang C, Wang H, Lai D, Rusli. High efficiency planar Si/organic heterojunction hybrid solar cells. Applied Physics Letters. 2012;**100**: 073503. DOI: 10.1063/1.3684872

[81] Xia Y, Zhang H, Ouyang J. Highly conductive PEDOT:PSS films prepared through a treatment with zwitterions and their application in polymer photovoltaic cells. Journal of Materials Chemistry. 2010;**20**:9740-9747. DOI: 10.1039/c0jm01593h

[82] Chiu WW, Travaš-Sejdić J, Cooney RP, Bowmaker GA. Studies of dopant effects in poly(3,4-ethylenedioxythiophene) using Raman spectroscopy. Journal of Raman Specroscopy. 2006;**37**:1354-1361. DOI: 10.1002/jrs.1545

[83] Tran-Van F, Garreau S, Louarn G, Froyer G, Chevrot C. Fully undoped and soluble oligo(3,4-ethylenedioxythiophene)s: Spectroscopic study and electrochemical characterization. Journal of Materials Chemistry. 2001;**11**:1378-1382. DOI: 10.1039/b100033k

[84] Garreau S, Louarn G, Buisson JP, Froyer G, Lefrant S. In situ spectroelectrochemical Raman studies of poly(3,4-ethylenedioxythiophene) (PEDT). Macromolecules. 1999;**32**: 6807-6812. DOI: 10.1021/ma9905674

[85] Sharma B, Fernanda Cardinal M, Kleinman SL, Greeneltch NG, Frontiera RR, Blaber MG, et al. High-performance SERS substrates: Advances and challenges. MRS Bulletin. 2013;**38**: 615-624. DOI: 10.1557/mrs.2013.161

[86] Ko H, Singamaneni S, Tsukruk VV. Nanostructured surfaces and assemblies as SERS media. Small. 2008;**4**:1576-1599. DOI: 10.1002/smll.200800337

[87] Lombardi JR, Birke RL, Lu T, Xu J. Charge-transfer theory of surface enhanced Raman spectroscopy. The Journal of Chemical Physics. 1986;**84**: 4174-4180. DOI: 10.1063/1.450037

[88] Li X, Zhang J, Xu W, Jia H, Wang X, Yang B, et al. Mercaptoacetic acid-capped silver nanoparticles colloid: Formation, morphology, and SERS

activity. Langmuir. 2003;**19**:4285-4290. DOI: 10.1021/la0341815

[89] Hao Z, Mansuer M, Guo Y, Zhu Z, Wang X. Ag-nanoparticles on UF-microsphere as an ultrasensitive SERS substrate with unique features for rhodamine 6G detection. Talanta. 2016; **146**:533-539. DOI: 10.1016/j.talanta.2015.09.024

[90] Bosnick K, Maillard M, Brus L. Single molecule Raman spectroscopy at the junctions of large Ag nanocrystals. The Journal of Physical Chemistry. B. 2003;**107**:9964-9972. DOI: 10.1021/jp034632u

[91] Tao A, Sinsermsuksakul P, Yang P. Tunable plasmonic lattices of silver nanocrystals. Nature Nanotechnology. 2007;**2**:435-440. DOI: 10.1038/nnano.2007.189

[92] Mulvihill MJ, Ling XY, Henzie J, Yang P. Anisotropic etching of silver nanoparticles for plasmonic structures capable of single-particle SERS. Journal of the American Chemical Society. 2010;**132**:268-274. DOI: 10.1021/ja906954f

[93] Jain PK, Lee KS, El-Sayed IH, El-Sayed MA. Calculated absorption and scattering properties of gold nanoparticles of different size, shape, and composition: Applications in biological imaging and biomedicine. The Journal of Physical Chemistry. B. 2006; **110**:7238-7248. DOI: 10.1021/jp057170o

[94] Mahmoud MA, El-Sayed MA. Different plasmon sensing behavior of silver and gold nanorods. Journal of Physical Chemistry Letters. 2013;**4**: 1541-1545. DOI: 10.1021/jz4005015

[95] Huang X, Neretina S, El-Sayed MA. Gold nanorods: From synthesis and properties to biological and biomedical applications. Advanced Materials. 2009; **21**:4880-4910. DOI: 10.1002/adma.200802789

[96] Halas NJ, Moskovits M. Surface-enhanced Raman spectroscopy: Substrates and materials for research and applications. MRS Bulletin. 2013;**38**: 607-611. DOI: 10.1557/mrs.2013.156

[97] Le F, Brandl DW, Urzhumov YA, Wang H, Kundu J, Halas NJ, et al. Metallic nanoparticle arrays: A common substrate for both surface-enhanced Raman scattering and surface-enhanced infrared absorption. ACS Nano. 2008;**2**: 707-718. DOI: 10.1021/nn800047e

[98] Fan JA, Wu C, Bao K, Bao J, Bardhan R, Halas NJ, et al. Self-assembled plasmonic nanoparticle clusters. Science. 2010;**328**:1135-1138. DOI: 10.1126/science.1187949

[99] Kho KW, Shen ZX, Zeng HC, Soo KC, Olivo M. Deposition method for preparing SERS-active gold nanoparticle substrates. Analytical Chemistry. 2005;**77**:7462-7471. DOI: 10.1021/ac050437v

[100] Lee CH, Hankus ME, Tian L, Pellegrino PM, Singamaneni S. Highly sensitive surface enhanced Raman scattering substrates based on filter paper loaded with plasmonic nanostructures. Analytical Chemistry. 2011;**83**:8953-8958. DOI: 10.1021/ac2016882

[101] Qu L-L, Li D-W, Xue J-Q, Zhai W-L, Fossey JS, Long Y-T, et al. Batch fabrication of disposable screen printed SERS arrays. Lab on a Chip. 2012;**12**: 876-881. DOI: 10.1039/C2LC20926H

[102] Yu WW, White IM. A simple filter-based approach to surface enhanced Raman spectroscopy for trace chemical detection. The Analyst. 2012; **137**:1168. DOI: 10.1039/c2an15947c

[103] Yu WW, White IM. Inkjet printed surface enhanced Raman spectroscopy array on cellulose paper. Analytical Chemistry. 2010;**82**:9626-9630. DOI: 10.1021/ac102475k

[104] Hulteen JC, Van Duyne RP. Nanosphere lithography: A materials general fabrication process for periodic particle array surfaces. Journal of Vacuum Science and Technology A. 1995;**13**:1553

[105] Zhang X, Whitney AV, Zhao J, Hicks EM, Van Duyne RP. Advances in contemporary nanosphere lithographic techniques. Journal of Nanoscience and Nanotechnology. 2006;**6**:1920-1934. DOI: 10.1166/jnn.2006.322

[106] Singh DP, Kumar S, Singh JP. Morphology dependent surface enhanced fluorescence study on silver nanorod arrays fabricated by glancing angle deposition. RSC Advances. 2015;**5**: 31341-31346. DOI: 10.1039/c5ra03225c

[107] Dick LA, McFarland AD, Haynes CL, Van Duyne RP. Metal film over nanosphere (MFON) electrodes for surface-enhanced Raman spectroscopy (SERS): Improvements in surface nanostructure stability and suppression of irreversible loss. The Journal of Physical Chemistry. B. 2002;**106**: 853-860. DOI: 10.1021/jp013638l

[108] Cinel NA, Cakmakyapan S, Butun S, Ertas G, Ozbay E. E-beam lithography designed substrates for surface enhanced Raman spectroscopy. Photonics and Nanostructures - Fundamentals and Applications. 2015; **15**:109-115. DOI: 10.1016/j.photonics.2014.11.003

[109] Jeong H-H, Mark AG, Gibbs JG, Reindl T, Waizmann U, Weis J, et al. Shape control in wafer-based aperiodic 3D nanostructures. Nanotechnology. 2014;**25**:235302. DOI: 10.1088/0957-4484/25/23/235302

[110] Gunnarsson L, Bjerneld EJ, Xu H, Petronis S, Kasemo B, Käll M. Interparticle coupling effects in nanofabricated substrates for surface-enhanced Raman scattering. Applied Physics Letters. 2001;**78**:802-804. DOI: 10.1063/1.1344225

[111] Fan M, Andrade GFS, Brolo AG. A review on the fabrication of substrates for surface enhanced Raman spectroscopy and their applications in analytical chemistry. Analytica Chimica Acta. 2011;**693**:7-25. DOI: 10.1016/j.aca.2011.03.002

[112] Le Ru EC, Etchegoin PG, Grand J, Félidj N, Aubard J, Lévi G, et al. Surface enhanced Raman spectroscopy on nanolithography-prepared substrates. Current Applied Physics. 2008;**8**: 467-470. DOI: 10.1016/j.cap.2007.10.073

[113] Kahl M, Voges E, Kostrewa S, Viets C, Hill W. Periodically structured metallic substrates for SERS. Sensors and Actuators B: Chemical. 1998;**51**: 285-291. DOI: 10.1016/S0925-4005(98)00219-6

[114] Hatab NA, Hsueh C-H, Gaddis AL, Retterer ST, Li J-H, Eres G, et al. Free-standing optical gold bowtie nanoantenna with variable gap size for enhanced Raman spectroscopy. Nano Letters. 2010;**10**:4952-4955. DOI: 10.1021/nl102963g

[115] Jen Y-J, Huang J-W, Liu W-C, Chan S, Tseng C-H. Glancing angle deposited gold nanohelix arrays on smooth glass as three-dimensional SERS substrates. Optical Materials Express. 2016;**6**:697. DOI: 10.1364/OME.6.000697

[116] Jen Y-J, Chan S, Huang J-W, Jheng C-Y, Liu W-C. Self-shadowing deposited pure metal nanohelix arrays and SERS application. Nanoscale Research Letters. 2015;**10**:498. DOI: 10.1186/s11671-015-1205-8

[117] Han Y-A, Ju J, Yoon Y, Kim S-M. Fabrication of cost-effective surface enhanced Raman spectroscopy substrate using glancing angle deposition for the detection of urea in body fluid. Journal of Nanoscience and Nanotechnology. 2014;**14**:3797-3799. DOI: 10.1166/jnn.2014.8184

[118] Abdulhalim I. Plasmonic sensing using metallic nano-sculptured thin films. Small. 2014;**10**:3499-3514. DOI: 10.1002/smll.201303181

[119] Singh JP, Chu H, Abell J, Tripp RA, Zhao Y. Flexible and mechanical strain resistant large area SERS active substrates. Nanoscale. 2012;**4**: 3410-3414. DOI: 10.1039/c2nr00020b

[120] Rajput A, Kumar S, Singh JP. Vertically standing nanoporous Al-Ag zig-zag silver nanorod arrays for highly active SERS substrates. Analyst. 2017; **142**:3959-3966. DOI: 10.1039/ C7AN00851A

[121] Namura K, Imafuku S, Kumar S, Nakajima K, Sakakura M, Suzuki M. Direction control of quasi-stokeslet induced by thermoplasmonic heating of a water vapor microbubble. Scientific Reports. 2019;**9**:4770. DOI: 10.1038/ s41598-019-41255-5

[122] Kumar S, Doi Y, Namura K, Suzuki M. Plasmonic nanoslit arrays fabricated by serial bideposition: Optical and surface-enhanced Raman scattering study. ACS Applied Bio Materials. 2020. Article ASAP, DOI: 10.1021/ acsabm.0c00215 [Accessed: 21 April 2020]

[123] Semin DJ, Rowlen KL. Influence of vapor deposition parameters on SERS active Ag film morphology and optical properties. Analytical Chemistry. 1994; **66**:4324-4331. DOI: 10.1021/ ac00095a032

[124] Chaney SB, Shanmukh S, Dluhy RA, Zhao YP. Aligned silver nanorod arrays produce high sensitivity surface-enhanced Raman spectroscopy substrates. Applied Physics Letters. 2005;**87**:031908. DOI: 10.1063/ 1.1988980

[125] Zhou Q, Li Z, Yang Y, Zhang Z. Arrays of aligned, single crystalline silver nanorods for trace amount detection. Journal of Physics D: Applied Physics. 2008;**41**:152007. DOI: 10.1088/ 0022-3727/41/15/152007

[126] Zhang ZY, Zhao YP. Tuning the optical absorption properties of Ag nanorods by their topologic shapes: A discrete dipole approximation calculation. Applied Physics Letters. 2006;**89**:23-25. DOI: 10.1063/1.2221403

[127] He Y, Larsen G, Li X, Ingram W, Chen F, Zhao Y. Nanoscale conical swiss roll with broadband visible and nir circular dichroism. Advanced Optical Materials. 2015;**3**:342-346. DOI: 10.1002/adom.201400435

[128] Mark AG, Gibbs JG, Lee TC, Fischer P. Hybrid nanocolloids with programmed three-dimensional shape and material composition. Nature Materials. 2013;**12**:802-807. DOI: 10.1038/nmat3685

[129] Titus J, Larsen G, Zhao Y, Perera AGU. Large circular dichroism and optical rotation in titanium doped chiral silver nanorods. Annals of Physics. 2016;**528**:677-683. DOI: 10.1002/andp.201600103

[130] Nair G, Singh HJ, Ghosh A. Tuning the chiro-plasmonic response using high refractive index-dielectric templates. Journal of Materials Chemistry C. 2015; **3**:6831-6835. DOI: 10.1039/ C5TC00922G

[131] Nair G, Singh HJ, Paria D, Venkatapathi M, Ghosh A. Plasmonic interactions at close proximity in chiral geometries: Route toward broadband chiroptical response and giant enantiomeric sensitivity. Journal of Physical Chemistry C. 2014;**118**: 4991-4997. DOI: 10.1021/jp4117535